*S. S. Abbas, T. McNally**

International Institute for Nanocomposite Manufacturing (IINM), WMG, University of Warwick, Coventry, UK

Composites of Cysteamine Functionalised Graphene Oxide and Polypropylene

Cysteamine functionalised reduced graphene oxide (rGO) was grafted to polypropylene-graft-maleic anhydride (PP-g-MA) and subsequently melt blended with PP. The covalent bridging of rGO to PP-g-MA via the cysteamine molecule and co-crystallization are routes to promoting interfacial interactions between rGO and the PP matrix. A rheological percolation threshold was achieved for a nanofiller loading between 3 wt% and 5 wt%, but none detected for the composites prepared with un-functionalized rGO. At low loadings (0.1 wt%), functionalized rGO is well dispersed in the PP matrix, an interconnecting filler-filler, polymer-filler and polymer-polymer network is formed, resulting in increased tensile toughness (1500%) and elongation at break (40%) relative to neat PP. Irrespective of whether the rGO was functionalised or not, it had a significant effect on the crystallization behavior of PP, inducing heterogeneous nucleation, increasing the crystallisation temperature (T_m) of PP by up to 10°C and decreasing the crystalline content (X_c) by ~30% for the highest (5 wt%) filler loading. The growth of the monoclinic α-phase of PP is preferred on addition of functionalised rGO and β crystal growth suppressed.

1 Introduction

The exceptional intrinsic properties of graphene(s) allows this material to be used in a wide array of applications as diverse as in energy storage devices (Foster et al., 2017), for biomedical purposes such as drug delivery (Sun et al., 2008) and also as a functional filler for polymer composites (Potts et al., 2011). It is widely reported both experimentally and from MD simulations (Zheng et al., 2007), that the dispersion of graphene in polymer matrices is critical in order to obtain a functional composite material. This becomes more so in the case of non-polar polyolefin matrices (e. g. polypropylene (PP) and polyethylene (PE)) as they tend to have limited interfacial interactions with graphene(s) due to low interaction energy between the two moieties (Lv et al., 2010). Appropriate functionalisation of the surfaces of graphene(s) will result in effective dispersion and distribution in polymer matrices and therefore enhancements in properties.

* Mail address: Tony McNally, International Institute for Nanocomposite Manufacturing (IINM), WMG, University of Warwick, Coventry CV4 7AL, UK
E-mail: t.mcnally@warwick.ac.uk

To overcome the incompatibility between non-polar polymers and graphene(s), a compatibilizer is required to promote interfacial interaction and permit interfacial stress transfer between the graphene and polymer. Many studies have reported the use of graft co-polymers as compatibilizers for composites of polymers and nanomaterials (Yetgin, 2020). Polypropylene-graft-maleic anhydride (PP-g-MA) is a common third component used to enhance mixing and adhesion between composite components. With the addition of PP-g-MA, compatibility between non-polar and polar entities are achieved as PP-g-MA locates to the interface with PP and encourages interfacial interaction through the chemical linking of the maleic anhydride groups with functionalities present on for example, graphene oxide (GO) (Lertwimolnun and Vergnes, 2005). Hsiao et al. (2011) introduced PP-g-MA to a diaminohexane functionalised thermally reduced graphene oxide (DAH-TRGO). Through an amidation reaction, the maleic anhydride groups of PP-g-MA and the amine groups on the functionalised TRGO surface were covalently linked prior to melt blending with PP. Nucleophilic reactions between primary amines and maleic anhydride groups of PP-g-MA chains have been reported widely and, rapidly yields amic acid and/or imid bonds during solution/melt blending (Li et al., 2017; Parija and Bhattacharyya, 2016; Yuan et al., 2014). Song et al. (2014) modified GO using bis(3-aminopropyl)-terminated poly(ethylene glycol) (NH_2-PEG-NH_2) and subsequently grafted with PP oligomer through reactive compatibilization. Through this GO modification, the free amines present react with the PP-g-MA resulting in better compatibility between the functionalised GO and the matrix. As a consequence improved thermal stability and flame retardant properties were obtained but, the crystallization behavior of PP was altered. Another approach described by Sanchez-Valdez et al. (2018), functionalised PP-g-MA with -[2-(dimethylamine)-ethoxy] ethanol (DMAE) in the melt to form PP-g-DMAE, again via an amination reaction. Composites of PP and GO were prepared by both solution and melt blending with the addition of PP-g-DMAE. PP-g-DMAE assisted exfoliation and dispersion of the GO within the polymer matrix resulting in significant improvements in mechanical, thermal and electrical properties.

In our previous work (Abbas et al., 2020a), we described the preparation and characterisation of the reaction between PP-g-MA and cysteamine modified reduced GO (rGO). Cysteamine was chosen to functionalise rGO as it is bi-functional, a thiol end group reacts with the double bonds of rGO (via a click reaction) and an amine end group reacts with the PP-g-MA once solution blended (via an amination reaction).

In that work, GO was reduced using hydrazine and then functionalised with cysteamine. The thiol end of the cysteamine molecule reacted with the double bonds of rGO using a thermal initiator (AIBN) and the amine was then further reacted with PP-g-MA to produce PP-g-MA-rGOcyst.

In this paper, we describe the preparation of composites of PP-g-MA-rGOcyst and PP, and investigate if the blend components are compatibilized by testing the hypothesis that the GO platelets are bound to PP-g-MA via the cysteamine molecule and the PP co-crystallizes with bulk PP. For comparative studies control samples were also produced without PP-g-MA and without cysteamine, and melt blended with bulk PP.

2 Experimental

2.1 Materials

PP (material grade 1063L1), melt flow rate (MFR): 8.0 g/10 min., was purchased from ExxonMobil (Machelen, Belgium) and used in pellet form. Graphene oxide (GO) (1 nm thick/size of flakes 2 to 20 µm) was purchased from Abalonyx, Oslo, Norway, polypropylene-graft-maleic anhydride (PP-g-MA) (average M_w ~9,100 by GPC and maleic anhydride 8 to 10 wt%), cysteamine hydrochloride (> 97.0%) and 2,2'-Azobis (2-methylpropionitrile) (AIBN) (98%) were purchased from Sigma Aldrich, Dorset, UK, and used as received. Sodium hydroxide pellets (> 97%), dimethylformamide (DMF), methanol, ethanol, toluene and ammonia were purchased from Fisher, and hydrazine hydrate (78 to 82%) from Honeywell Fluka, Rugby, UK, and all used as received.

2.2 Synthesis of PP-g-MA-rGOcyst

To prepare PP-g-MA-rGO-cyst, GO was first reduced using hydrazine and ammonia and then functionalised with cysteamine using AIBN as thermal initiator. The rGO-cysteamine was then solution blended with PP-g-MA in toluene at reflux conditions (120 °C) for 24 h under N_2. For more details on preparation and characterisation see our previous publication (Abbas et al., 2020a). The mixture was then washed with methanol repeatedly using hot filtration with a 0.2 µm polytetrafluoroethylene (PTFE) membrane. The product was dried in a vacuum oven at 80 °C overnight to yield PP-g-MA-rGO-cyst.

2.3 Composite Preparation

PP pellets were first cryo-milled to form a powder using a SPEX SamplePrep Freezer Mill (Stanmore, UK). These PP pellets were cooled for 10 min using liquid nitrogen, followed by 2 × 10 min grinding cycles at 15 Hz. In between each cycle the samples were allowed to cool for a 5 minute interval. The resultant PP powder was then dried in a vacuum oven at 40 °C for 24 h before processing. Composites were prepared using the following amounts of polymer (see Table 1) and modified GO so as to achieve 0.1, 0.5, 1.0 and 5.0 wt% GO loading. The components were first dry-blended and then melt-blended using a laboratory scale extruder (model Haake Lab, Thermo Scientific, Waltham, MA, USA), equipped with twin conical screws (non-modular, screw diameter = 5/14 mm (conical), screw length = 109.5 mm) at 170 °C. After melting, each composition was then fed directly into a microinjection molding machine (model Multijet Plus, Thermo Scientific, Waltham, MA, USA)

Nomenclature	PP wt%	PP(x)-g-MA(y) wt% x:y	rGO wt%	rGO-cyst wt%*
PP	100			
PP/NF (0.1)	99.9		0.1	
PP/NF (0.5)	99.5		0.5	
PP/NF (1.0)	99.0		1.0	
PP/NF (3.0)	97.0		3.0	
PP/NF (5.0)	95.0		5.0	
PP/C/NF (0.1)	99	0.8:0.1	0.1	
PP/C/NF (0.5)	95	4:0.5	0.5	
PP/C/NF (1.0)	90	8.0:1.0	1.0	
PP/C/NF (3.0)	75	24:3	3.0	
PP/C/NF (5.0)	50	40:5	5.0	
PP/C/NF-F (0.1)	99	0.8:0.1		0.1
PP/C/NF-F (0.5)	95	4:0.5		0.5
PP/C/NF-F (1.0)	90	8.0:1.0		1.0
PP/C/NF-F (3.0)	75	24:3		3.0
PP/C/NF-F (5.0)	50	40:5		5.0

*Refers to rGO content (wt%) only

Table 1. Nomenclature and composition of blends studied

to yield standard dumbbell-shaped specimens according to ASTM D68 V for tensile testing and disk shaped samples (d = 25 mm, h = 1.5 mm) for oscillatory rheology and X-ray diffraction measurements. The injection and mold temperatures were set to 190 °C and 100 °C, respectively with the injection pressure = 200 bar and post pressure of 100 bar for 10 s. For simplicity, the following blend nomenclature is adopted; bulk PP=PP, rGO=NF (nanofiller), rGOcyst=NF-F (functionalised NF) and PP-g-MA=C (compatabilizer).

2.4 Characterisation

For tensile testing (10 replicates), a autograph AGS-X frame (Shimadzu, Kyoto, Japan) was used. This was equipped with a 10 kN load cell with a twin TRIViewX noncontact digital video extensometer (500 and 120 mm field view), Shimadzu Corp., Kyoto, Japan. Data was captured using Trapezium X version 1.4 software package (Shimadzu Corp., Kyoto, Japan), and the samples tested were standard dumbbell-shaped test specimens with an extensometer gauge length of 7.62 mm and a constant crosshead speed of 10 mm/min. The total mechanical energy consumed by the material when straining it to break per unit volume was used as a measurement for the tensile toughness (W_b) of a material. This value can be extrapolated by integrating the area under stress-strain curves using the following equation (Van Vlack, 1989):

$$W_b = \int_0^{\varepsilon} \sigma d\varepsilon.$$

Dynamic mechanical thermal analysis (DMTA) was carried out in the dual cantilever mode with a free length of 17.50 mm, sample width of 10 mm and thickness of 4 mm using a Triton Tritec 2000 DMA (Triten Technology Ltd., Leicester, UK) equipped with a standard oven.

A rheometer with parallel-plate geometry (model Haake Mars III, Thermo Scientific, Waltham, MA, USA) was used to measure the rheological behavior of the composites. These samples first underwent oscillatory amplitude stress sweeps over a stress range of 0.1 to 100 Pa at a fixed temperature and frequency of 185 °C and 1 Hz, respectively. This determined that at 10 Pa the storage modulus is independent of deformation; frequency scans were performed from 0.1 to100 Hz under a controlled stress of 10 Pa in an air atmosphere.

X-ray diffraction measurements were performed on a 3rd generation instrument equipped with multicore (iCore/dCore) optics and a Pixcel3D detector operating in 1D scanning mode (all Malvern Panalytical Empyrean, Malvern, UK). A Cu tube was used giving Cu $K\alpha_{1/2}$ radiation (1.5419 Å) and a beam knife was used to reduce air scatter at the low angles. Scans were made in the range 4° to 40° 2θ with a step size of 0.0263° and a counting time of ~ 130s/step.

Differential Scanning Calorimetry (DSC) was performed using a DSC1 (model 700, 400 W, Mettler Toledo, Leicester, UK) and the data collected and evaluated using a STARe Version 15.01 software package (Mettler Toledo, Leicester, UK). The samples were studied between 25 °C and 200 °C at a heating and cooling rate of 10 K/min for two cycles. The thermograms were used to determine the melt temperature (T_m), crystallisation temperature (T_c), enthalpy of melting (ΔH_m), enthalpy of crystallisation (ΔH_c) and the percentage crystallinity (X_c) of PP. The crystallinity was calculated by dividing the ΔH_m or ΔH_c for the sample by the theoretical 100 % crystalline value for PP (ΔH_f: 209 J/g) (Dechant, 1990) and allowing for blend composition.

Scanning electron microscopy (SEM) images were obtained using a field emission instrument (model Zeiss Sigma, Zeiss, Oberkochen, Germany). Tensile dumbbell specimens were cryo-fractured by placing them in a bath of liquid nitrogen for 30 min and then striking them. The fractured surfaces were attached to aluminium SEM stubs using carbon adhesive tape with the fractured surface facing upward. The samples were also sputter coated (10 nm) with a Au/Pt metal target (Cressington 108 auto) to minimize charging effects.

3 Results and Discussion

The inclusion of C in both PP/C/NF and PP/C/NF-F composites is expected to alter the PP chain dynamics and the viscoelastic properties of the composites as seen in the rheology results plotted in Fig. 1. An increase in storage modulus (G') was observed for PP/C/NF-F composites with increasing NF-F loading, at lower frequencies. This increase is associated with the strong interactions between the NF-F and the C, the uniform distribution of C-NF-F within the PP matrix and the enhanced interfacial interaction between the NF-F with the polymer (Bai et al., 2019). This increase in G' shows that the C/NF-F contributes more to the elasticity than the viscous nature of the polymer composite (Mun et al., 2014). For the 5.0 wt% loading, some shear thinning behavior was observed even at low frequencies. This transition from 'liquid-like' to more 'solid-like' behavior at lower frequency is a consequence of the interconnected network formed hindering polymer chain dynamics (Abbas et al., 2020b). Further evidence for the formation of a percolated network was seen from a plot of tan δ versus frequency. A transition to more 'solid-like' behavior results in a decrease in tan δ, as seen for the PP/C/NF-F composites. For unfilled PP and the composites with low C/NF-F loading, from 0.1 to 1.0 wt%, an increase in tan δ was obtained. In contrast, for composites with C/NF-F loading of 3.0 and 5.0 wt%, tan δ decreases significantly at lower frequency, forming a plateau suggesting that percolation was reached at some loading between 3.0 and 5.0 wt% C/NF-C (McClory et al., 2010).

However, it is more correct to construct Cole-Cole (G′ vs. G″), Han (η′ vs. η″) and Van Gurp-Palmen (δ versus G*) plots to asses if percolation has been achieved, see Fig. 2. If increasing the C/NF-F loading results in more 'solid-like' behavior and the formation of a percolated filler-filler and/or filler-polymer network, then the associated changes in the viscoelastic behavior of the polymer will be obvious from these plots (Nobile, 2011). In the Cole-Cole plot (Fig. 2A) the deviation in the linear relationship between G′ vs. G″ can be interpreted as a transition to either more 'liquid-like' or solid-like' behavior. For C/NF-F loadings up to 1.0 wt%, the plots for the composites of G′ vs. G″ directly overlap that of unfilled PP. However, as the C/NF-F content increases up to 5 wt% these curves are no longer superimposed on the PP curve and clearly show the onset of the formation of a percolated network at 3 wt% C/NF-F. The value of G′ for any given G″ was higher for the 3.0 wt% and 5.0 wt% composites as these composites are more elastic than unfilled PP (Chin et al., 2015). The Han plots in Fig. 2B show the imaginary (loss) viscosity (η″) and relative

(real) viscosity (η′) where neat PP exhibits a semi-circle shaped curve, behavior attributed to the mechanisms of relaxation of the polymer chains. The composites with low C/NF-F loadings (< 3 wt%) show similar trends to that of the unfilled PP, whereas at loadings ≥ 3 wt% the composites start to exhibit a more linear relationship between real viscosity versus the loss viscosity. This sudden increase in η′ between 3 and 5 wt% C/NF-F further confirms the transition to more 'solid-like' behavior and increased polymer relaxation times as a consequence of the formation of a filler-filler and filler-polymer network (Gupta et al., 2017). In this instance, the increased interactions between NF and NF and NF and PP are achieved via the covalently bonding with C resulting in an interconnected percolated network which delays polymer relaxation processes (Bai et al., 2019). This conclusion is further supported from the Van Gurp-Palmen plot (i.e. Figure 2C, δ versus G*) for these composites, where generally the phase angle (δ) of an ideal elastic solid is 0° and for an ideal viscous fluid 90°. Therefore, for a more elastic ('solid-like') material, usually lower values of δ are measured (Bai et al., 2019). For neat PP and the composites with ≤ 1.0 wt% C/NF-F, the dynamics of the PP chains is not greatly altered, therefore in the lower G* region (10^2 to 10^3 Pa), δ is between 80° and 90°, more 'liquid-like' or viscous flow is dominant (Chiu et al., 2016). For composites with > 3 wt% C/NF-F, in the same G* region, δ decreases to as low as 63.4° for the 5.0 wt% composite, i.e. enhanced elastic behavior of the composites.

The onset of a rheological percolation starts around 3.0 wt% and a percolated network has clearly formed at some C/NF-F loading between 3.0 and 5.0 wt%.

This behavior is clearly associated with the formation of an interconnected PP/C/NF-F network, which is not observed for

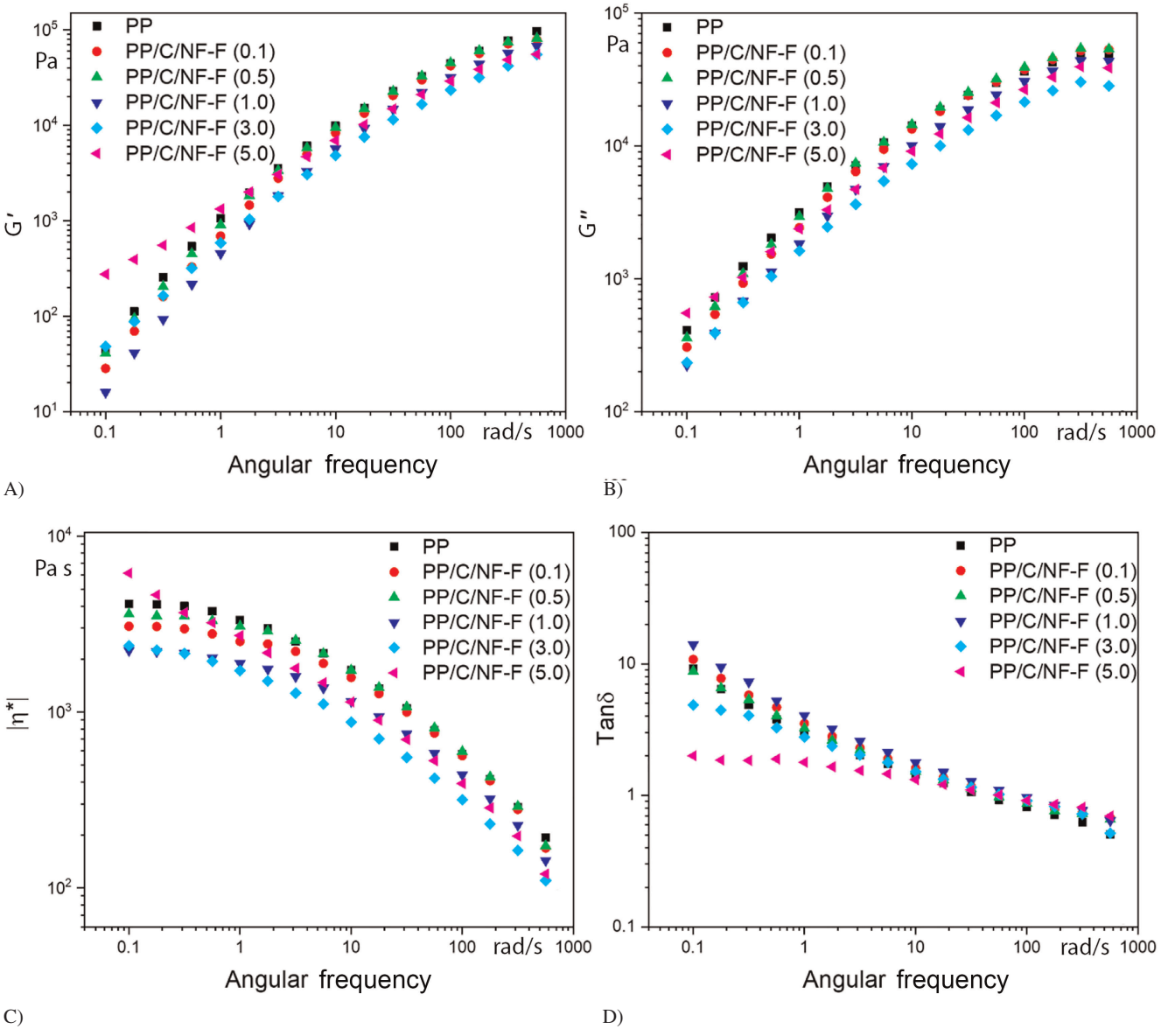

Fig. 1. Variation in (A) storage modulus (G′), B) loss modulus (G″), C) complex viscosity (η) and D) tan δ as a function of angular frequency (ω) for neat PP and PP/C/NF-F composites*

the PP/NF and PP/C/NF composites, i.e. without cysteamine functionalisation, at similar filler loadings (> 3 wt%). The evidence for the formation of percolated networks can be seen by comparing the Cole-Cole, Han and Van Gurp-Palmen plots for all three sets of composites, PP-NF, PP/C/NF and PP/C/NF-F, see Fig. 3. No evidence for percolation was obtained for the PP/NF composites, rather a behavior similar to that of neat PP. In contrast, when C and or NF-F are added to the bulk PP at >3 wt%, the deviation obtained in the relationship between G′ vs G″, δ vs |G*| and η″ vs η′ are responses indicative of a percolated network. These changes show that the presence of NF alone is not effective at creating a percolated network in PP, but functionalisation with cysteamine (NF-F) is required and achieved by covalently linking the PP-g-MA (C) and rGO (NF) to produce C/NF-F, which in turn is more compatible with PP than C/NF or NF alone.

The strong nucleating effect that graphene(s), including GO, have for PP is well documented and the role, if any, of cysteamine functionalisation was investigated by DSC and XRD. Figure 4 shows the first and second DSC heating and cooling cycles for the PP/C/NF-F composites. The relevant thermal parameters for all composites were determined and listed in Table 2. As expected, neat (unfilled) PP displays one relatively sharp peak, with a melting peak (T_m) at 167 °C. However, the extruded composites exhibit a broader, less intense melting transition peak, with T_m decreasing with increasing C/NF loading down to 156 °C, associated with the melting of both PP α and β crystallites. The decrease in T_m is less when the NF is functionalised with cysteamine (NF-F), down to 160 °C. Increasing anhydride content within the composites also results in a reduction in T_m and a broadening of the crystallisation peaks (Menyhárd et al., 2008). The depression of the melting peak and T_m and the absence of a distinct T_m peak for C suggests that the crystalline region of C has co-crystallized with the isotactic PP (Harper et al., 2009). Furthermore, X_c increases from 48 % for the neat PP to 55 % with just the addition of 0.1 wt% PP/C/NF-F. Overall, X_c for the composites was higher than that for neat PP, the presence of NF-F and C initiated heterogeneous nucleation. However, at the highest loadings studied (5 wt%), X_c drastically decreases to 38 %, as the increased PP-g-MA(C) and NF/NF-F content that formed a percolated network hinders polymer chain dynamics and conformational change, limiting crystal growth (Martínez-

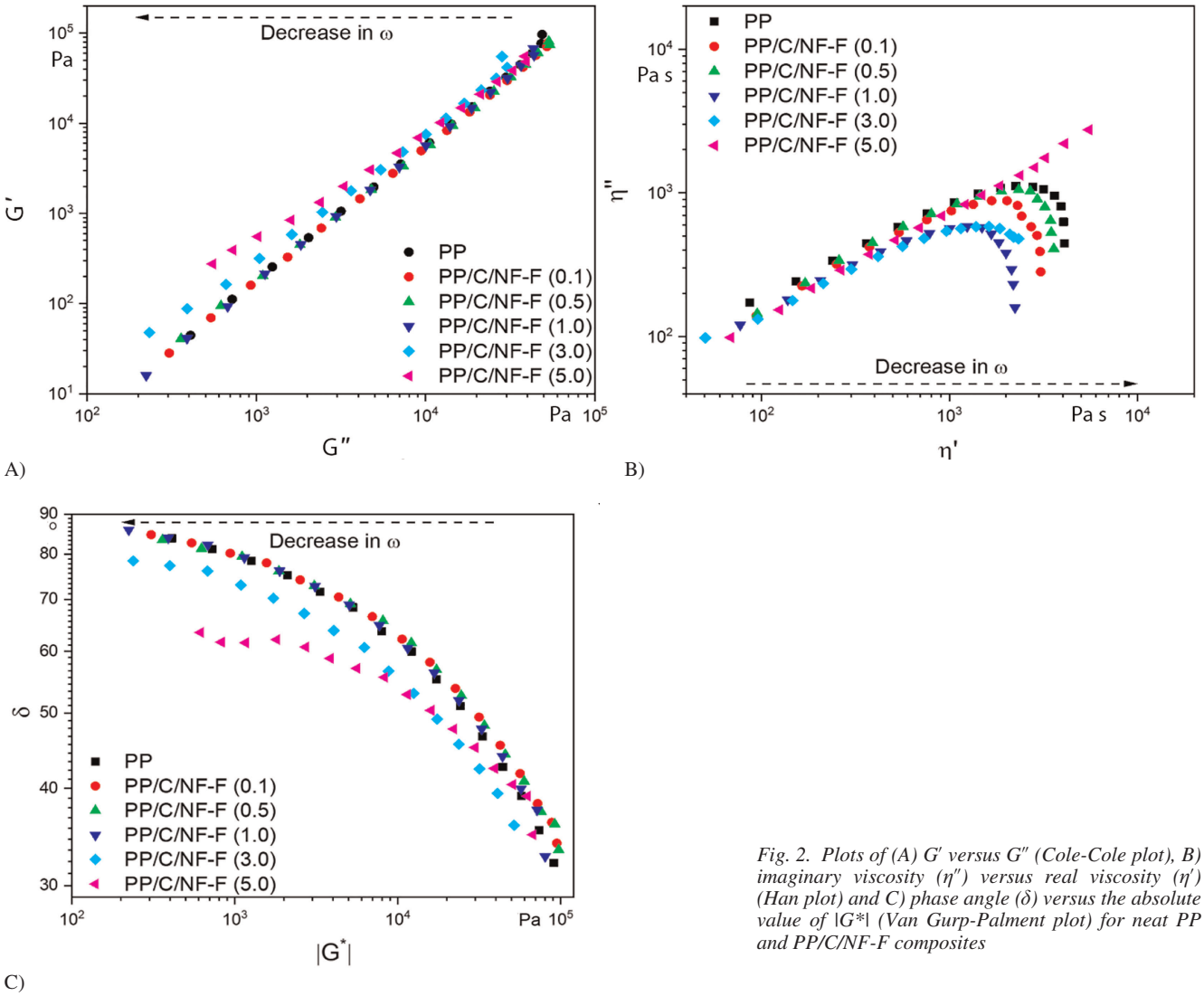

Fig. 2. Plots of (A) G′ versus G″ (Cole-Cole plot), B) imaginary viscosity (η″) versus real viscosity (η′) (Han plot) and C) phase angle (δ) versus the absolute value of |G| (Van Gurp-Palment plot) for neat PP and PP/C/NF-F composites*

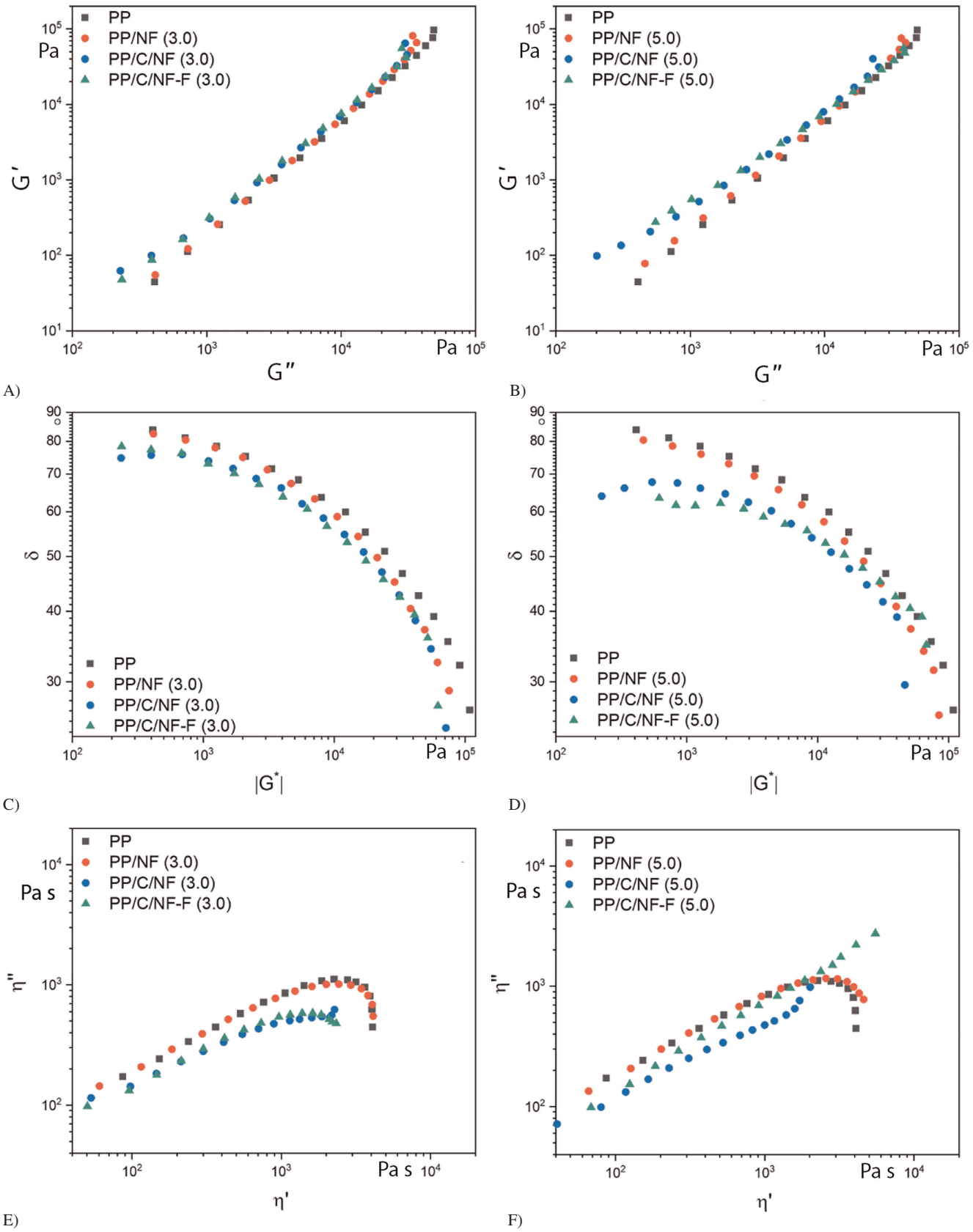

Fig. 3. Cole-Cole (G′ vs. G″), Van Gurp-Palmen (δ vs. |G|) and Han (η″ vs. η′) plots for neat PP, 3 wt% (A, C, E) and 5 wt% (B, D, F) PP/NF, PP/C/NF and PP/C/NF-F composites*

Colunga et al., 2018). Additionally, with increasing C/NF-F content, the crosslink density increases altering crystallisation behavior. In contrast, are for NF loadings < 5 wt%, X_c and ΔH_c is higher than for neat PP, suggesting a strong nucleating effect where a PP phase crystallises on the NF surface (Khare et al., 2011; Parija and Bhattacharyya, 2016). Tc increases by as much as 10 °C. The super cooling values ($\Delta T = T_m - T_c$) have also been listed in Table 2 and ΔT decreases for all composites relative to neat PP, which is a strong evidence for a higher nucleation and crystallisation rate. Both PP/C/NF and PP/C/NF-F have lower ΔT values relative to the PP/NF highlighting the role that the compatibilized NF (C/NF-F) plays in nucleation, increasing the rate of crystallization, promoting interfacial interaction between the NF and PP and PP crystallization on the NF surface (Kalantari et al., 2015a).

Clearly, inclusion of both NF and NF-F altered the crystallisation behavior of PP. This relationship was investigated further by XRD, as the width of the diffraction peak can be related to the apparent crystal size (ACS) calculated from the Scherrer equation:

$$ACS = \frac{K\lambda}{\beta_0 \cos\theta}, \quad (1)$$

where K is a constant and refers to how the width is calculated (0.94), λ is the wavelength of radiation (0.15419 nm), β_0 is the full-width at half-maximum intensity of a pure equatorial reflection in radians (FWHM) and θ is the diffraction angle in radians (Murthy, 2016). Additionally, the fraction of PP β-phase formed (K_β) for the composites can be calculated using Eq. 2:

$$K_\beta = \frac{H_\beta}{H_\beta + H_{\alpha 1} + H_{a2} + H_{a3}}, \quad (2)$$

where H_β is the intensity of the β (300) peak and $H_{\alpha 1}$, $H_{\alpha 2}$ and $H_{\alpha 3}$ are the intensities of the α (100), α (040) and α (130) peaks,

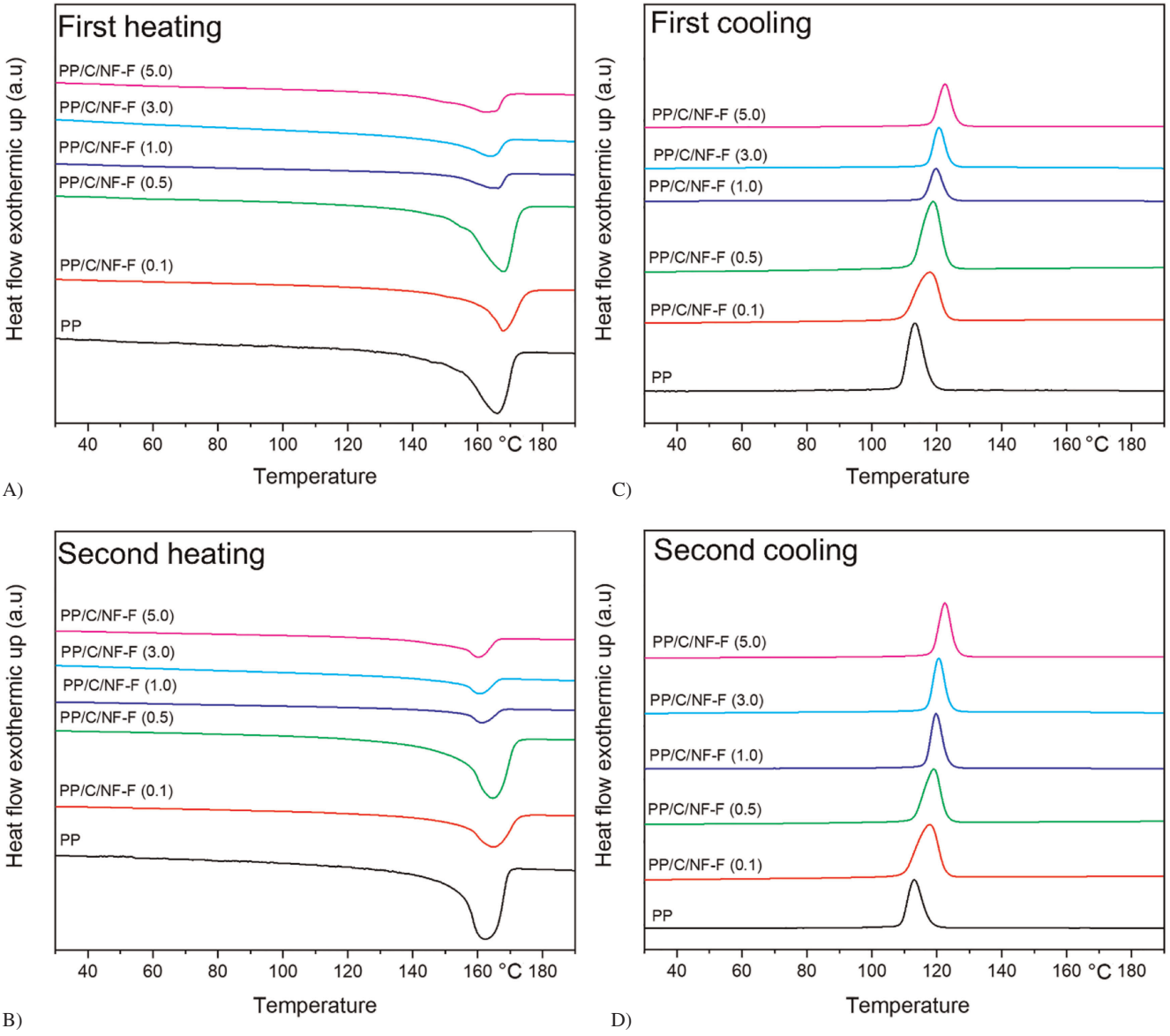

Fig. 4. First and second heating cycles (A, B) and first and second cooling cycles (C, D) for PP and PP/C/NF-F composites

respectively (Huo et al., 2004; Juhász et al., 2002). All values are listed in Table 3. Figure 5 shows the XRD patterns for neat PP relative to the PP/NF, PP/C/NF and PP/C/NF-F composites. For neat PP, the α crystalline peaks were seen at 2θ: 13.81° (100), 16.57° (040), 18.23° (130) and 20.77° and 21.51° (111)+(301). Additionally, a strong β peak was also recorded at 2θ: 15.77° for the β (300) for neat PP, showing the polymorphism of the PP used in this study. Without the inclusion of C, i.e. for the PP/NF composites, a general decrease in FWHM was observed for the (100), (300) and (040) crystal planes. For the (100) crystal plane, a decrease in FWHM with increasing NF loading was measured, which resulted in an increase in ACS relative to neat PP (20.25 nm). Additionally, a general decrease in K_β (%) was also exhibited with the addition of NF to PP as the NF acts as an effective α-nucleating agent increasing the α crystallite size and crystallinity (DSC) and decreasing the amount of β crystallite formed. When C is included (PP/C/NF), a further decrease in K_β (%) was obtained, showing that both NF and C act as a β polymorph suppressant. Additionally, the ACS for the (100) crystal plane increased for NF loadings ≤ 0.5 wt% followed by a decrease at higher loadings > 1 wt% relative to neat PP. Similar trends for the FWHM values for these compositions were observed. For the PP/C/NF composites, K_β (%) is significantly decreased due to suppres-

Sample	ΔH_m J g^{-1}	ΔH_c J g^{-1}	T_m °C	T_c °C	X_c %	$\Delta T = T_m - T_c$ °C
PP	78	69	167	113	48	54
PP/NF (0.1)	107	102	162	118	49	44
PP/NF (0.5)	108	98	161	121	46	40
PP/NF (1.0)	110	108	162	121	51	41
PP/NF (5.0)	110	100	164	123	45	41
PP/C/NF (0.1)	102	94	164	117	45	47
PP/C/NF (0.5)	76	78	162	118	47	44
PP/C/NF (1.0)	102	103	162	120	48	42
PP/C/NF (3.0)	91	90	162	121	41	41
PP/C/NF (5.0)	77	79	156	119	34	37
PP/C/NF-F (0.1)	89	105	165	118	55	48
PP/C/NF-F (0.5)	108	105	165	119	50	47
PP/C/NF-F (1.0)	88	97	161	120	54	42
PP/C/NF-F (3.0)	97	134	161	121	54	41
PP/C/NF-F (5.0)	89	87	160	122	38	38

Table 2. Thermal parameters for neat PP, PP/NF, PP/C/NF and PP/C/NF-F composites determined from DSC measurements

Sample	FWHM (100) °	FWHM (300) °	FWHM (040) °	ACS (100) nm	ACS (040) nm	ACS (300) nm	K_β %
PP	0.41	0.29	0.42	20.25	19.75	28.86	31.60
PP/NF (0.1)	0.37	0.29	0.36	22.41	23.10	23.08	15.43
PP/NF (0.5)	0.36	0.28	0.36	23.05	23.15	23.13	28.61
PP/NF (1.0)	0.34	0.28	0.36	24.65	23.40	23.37	24.23
PP/NF (3.0)	0.39	0.31	0.38	21.38	22.32	22.30	23.77
PP/NF (5.0)	0.33	0.31	0.36	25.16	23.23	23.21	13.88
PP/C/NF (0.1)	0.39	0.49	0.38	21.54	22.33	17.21	10.47
PP/C/NF (0.5)	0.40	0.36	0.40	20.67	20.73	23.17	18.23
PP/C/NF (1.0)	0.55	0.62	0.45	15.07	18.48	13.62	19.70
PP/C/NF (3.0)	0.48	0.63	0.42	17.39	19.81	13.27	15.60
PP/C/NF (5.0)	0.68	0.71	0.40	12.23	20.76	11.80	12.64
PP/C/NF-F (0.1)	0.44	0.41	0.42	19.14	20.02	20.29	15.63
PP/C/NF-F (0.5)	0.36	0.29	0.37	23.01	22.48	29.12	17.82
PP/C/NF-F (1.0)	0.44	0.56	0.41	18.99	20.32	14.87	11.63
PP/C/NF-F (3.0)	0.34	0.53	0.35	24.24	23.88	15.75	8.88
PP/C/NF-F (5.0)	0.48	0.47	0.41	17.25	20.39	17.73	16.32

Table 3. FWHM and ACS values calculated from XRD peaks for (100), (300), and (040) crystal planes. K_β values tabulated for neat PP, PP/NF, PP/C/NF and PP/C/NF-F composites

sion of the formation of the β polymorph on inclusion of both NF and C together. The general trend for the PP/C/NF-F composites is an increase in ACS for the (100) and (040) planes and a decrease in ACS for the β (300) plane. The covalently bound C-NF-F within the PP matrix results in preferential growth of the monoclinic α-phase of PP and suppressing β crystals growth, seen by the decrease in K_β (%). Additionally, the α-form is attributed to brittle behavior while the β-form is associated with more ductile behavior for PP (De Rosa, Scoti, Di Girolamo, de Ballesteros, Auriemma and Malafronte 2020).

Representative stress-strain curves from static tensile testing of the composites relative to neat PP are shown in Fig. 6. For the PP/NF composites, an increase in strain at break (ε_B) is recorded at the lower NF loading (≤ 0.5 wt%), but at higher loadings the composite exhibits lower values of strain, as it is more brittle. This is a common observation with poorly dispersed unfunctionalised graphene(s) in non-polar polymers, as with increasing NF content, NF agglomerations act as stress concentration points in the PP matrix. When C is added to PP/C/NF, the lowest NF loading (0.1 wt%) gives the highest ε_B relative to neat PP, an increase of about 50 %. With increasing NF loading in PP/C/NF, the composites become brittle even more so than neat PP. The presence of C 'plasticizes' the matrix, making it more ductile but, with increasing NF content, agglomeration dominates causing embrittlement of the composite. Finally, for the PP/C/NF-F composites, a significant enhancement in ε_B for the 0.1 wt% loading is obtained, up to about 600 %. At this loading, the cysteamine functionalised rGO (NF-F) binds with C covalently, facilitating more effective interfacial interaction between the NF-F and the PP matrix. Without the covalent attachment, the composite at the same 0.1 wt% loading is also more ductile than neat PP, but not to the same level as to when C is included.

In addition, values for Young's modulus (E), tensile strength (σ), tensile toughness (W_b) and strain at break (ε_B) for neat PP and PP/C/NF-F, PP/C/NF and PP/NF composites were determined and are shown graphically in Fig. 7. For PP/NF, no significant changes were seen in σ and only a modest increase E at the highest (5 wt%) NF loading, relative to neat PP. After addition of C, to form PP/C/NF or P/C/NF-F composites, σ was

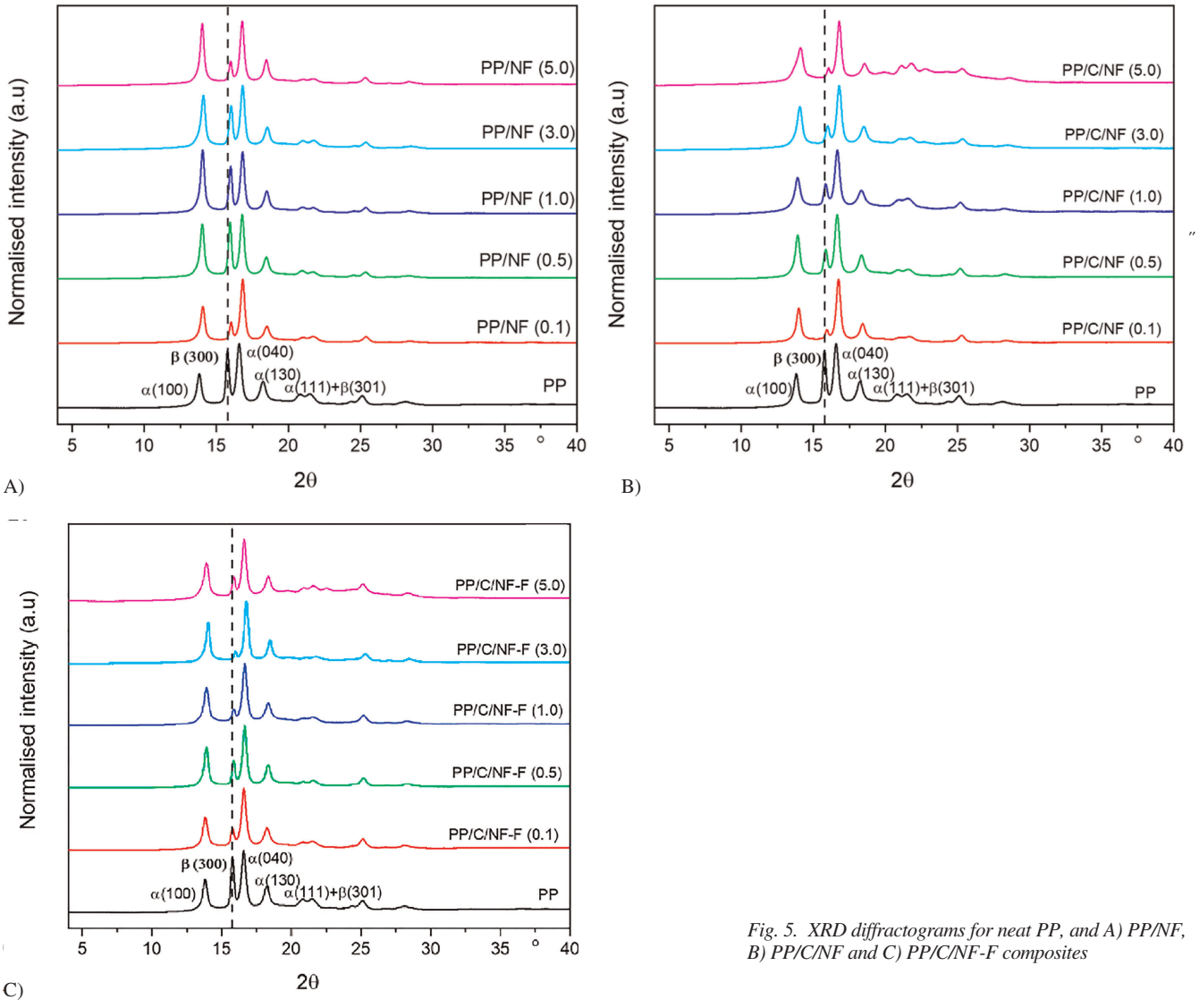

Fig. 5. XRD diffractograms for neat PP, and A) PP/NF, B) PP/C/NF and C) PP/C/NF-F composites

similar to neat PP and all other composites. A similar trend was obtained for E, except at the 5 wt% C/NF-F loading, when σ was about 40 % than for both unfilled PP and all other composites. Most interesting was the significant increase in tensile toughness (W_b) by about 1 500 % and ε_B (as described above) when the C/NF-F loading was just 0.1 wt%. It may be that a combination of a highly dispersed NF-F component at this low loading covalently bonded to C results in major increases in tensile toughness and ductility (Liu et al., 2016). With further successive increases in NF-F loading, a significant drop in W_b and ε_B is obtained.

From DMTA measurements, PP displays three dynamic relaxations in a plot of tan δ versus temperature, α, β and γ. The α-relaxation is attributed to lamellar slip and rotation within the crystalline phase, typically observed at ~60 °C. The β-relaxation, derived from the dynamic glass-rubber transition of the PP amorphous phase, occurs between –20 °C and +20 °C. Finally, the γ-relaxation is associated with the mobility of a few chain segments existing in the amorphous region of the semi-crystalline polymer at –50 °C, but is often not observed (Kotsilkova et al., 2010). In this study, the storage modulus (E′) for all the composites decreased drastically, especially at the glass transition temperature (T_g, –15 °C to 25 °C), classically associated with the polymer chains having higher molecular mobility above T_g, (Fig. 8). As expected, as the wt% of C/NF-F increases, an increase in E′ is recorded relative to unfilled PP, by about one order of magnitude at the 5 wt% level from a stiffer interphase region between the NF-F and PP/C system (Ardanuy et al., 2010). This interface/interphase forms more readily for the PP/C/NF-F composites due to the improved compatibility between the PP matrix and NF. The loss modulus (E″) curves for the PP/C/NF-F composites were less intense than those for the other composites, the viscous damping is lower as is the dissipation capacity of the material (Benmesli and Riahi, 2014), the composite is more stiff and polymer chains less mobile. Additionally, the difference in intensity of the main peak in the tan δ plot (going through the T_g) suggests different molecular relaxations exhibited by the neat PP, PP/NF and PP/C/NF to PP/C/NF-F composites, see Table 4. The greater damping displayed by neat PP, PP/NF and PP/C/NF

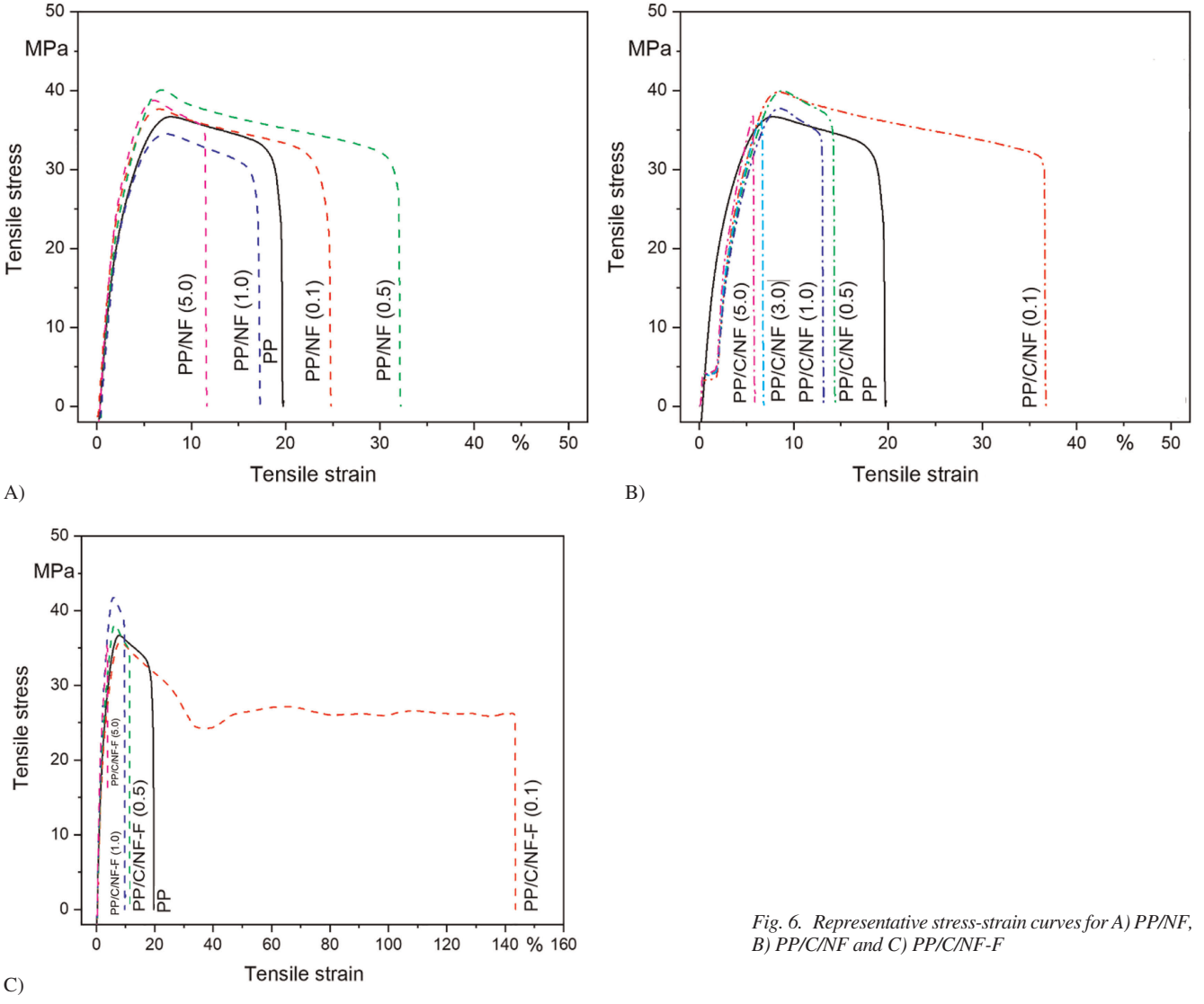

Fig. 6. Representative stress-strain curves for A) PP/NF, B) PP/C/NF and C) PP/C/NF-F

composites relative to PP/C/NF-F at T_g is derived from a non-percolated, non-interconnected polymer-filler network. The network formed via C/NF-F hinders polymer chain dynamics, resulting in an increase in the elastic response of the matrix and therefore lowering the damping characteristics (Kalantari et al., 2015b). For the PP/C/NF composites, the NF is not bound to cysteamine (F) and therefore C is not covalently bonded to NF, an increase in tan δ is seen at T_g and the T_g decreases with increasing NF loading, see Table 4. Additionally, all other composites had lower E′ relative to the PP/C/NF-F composites. This decrease in T_g values for the composites containing C may be derived from a plasticizing effect where increased polymer chain mobility shifts the glass transition to lower temperatures (Létoffé et al., 2019).

It is clear that C/NF-F promotes compatibilization of GO (NF) and PP and NF dispersion in the polymer. The reaction of C with NF-F seems to provide some degree of wetting between the NF and matrix by coating the GO (NF) platelets, see SEM images in Figs. 9A and B. Moreover, the inclusion of C and the formation of C/NF-F helps to partially exfoliate the GO (NF) layers, Figs. 9C, D and E. This can be seen clearly in e) where the C/NF-F (circled in red) is located between the layers, but distributed widely.

The inclusion of C/NF-F in PP gives rise to three different interactions, which in turn determine the properties of these composites. Our physical interpretation of these interactions is given schematically in Fig. 10. They are, i) polymer-polymer interactions, i.e. between the PP chains of PP-g-MA and the

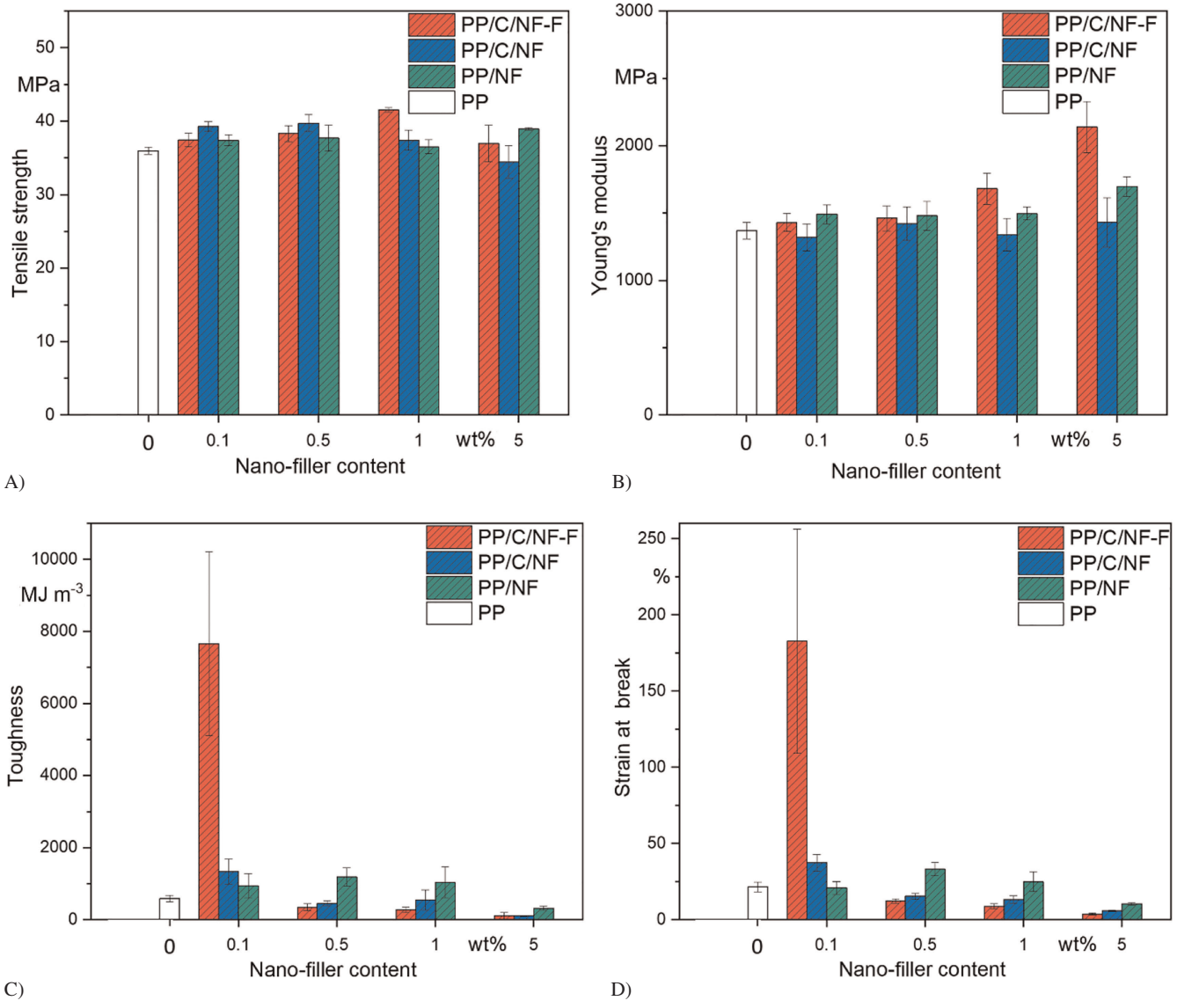

Fig. 7. Variation in (A) tensile strength (σ), B) Young's modulus (E), C) tensile toughness (W_b) and D) strain at break (ε_B) for neat PP, PP/NF, PP/C/NF and PP/C/NF-F composites

PP matrix via co-crystallization, ii) interaction between C and NF-F covalently bound by the cysteamine (F) and iii) the interaction between PP, C and NF-F. The different roles C plays are most obvious at the 5 wt% C/NF-F loading given the change in

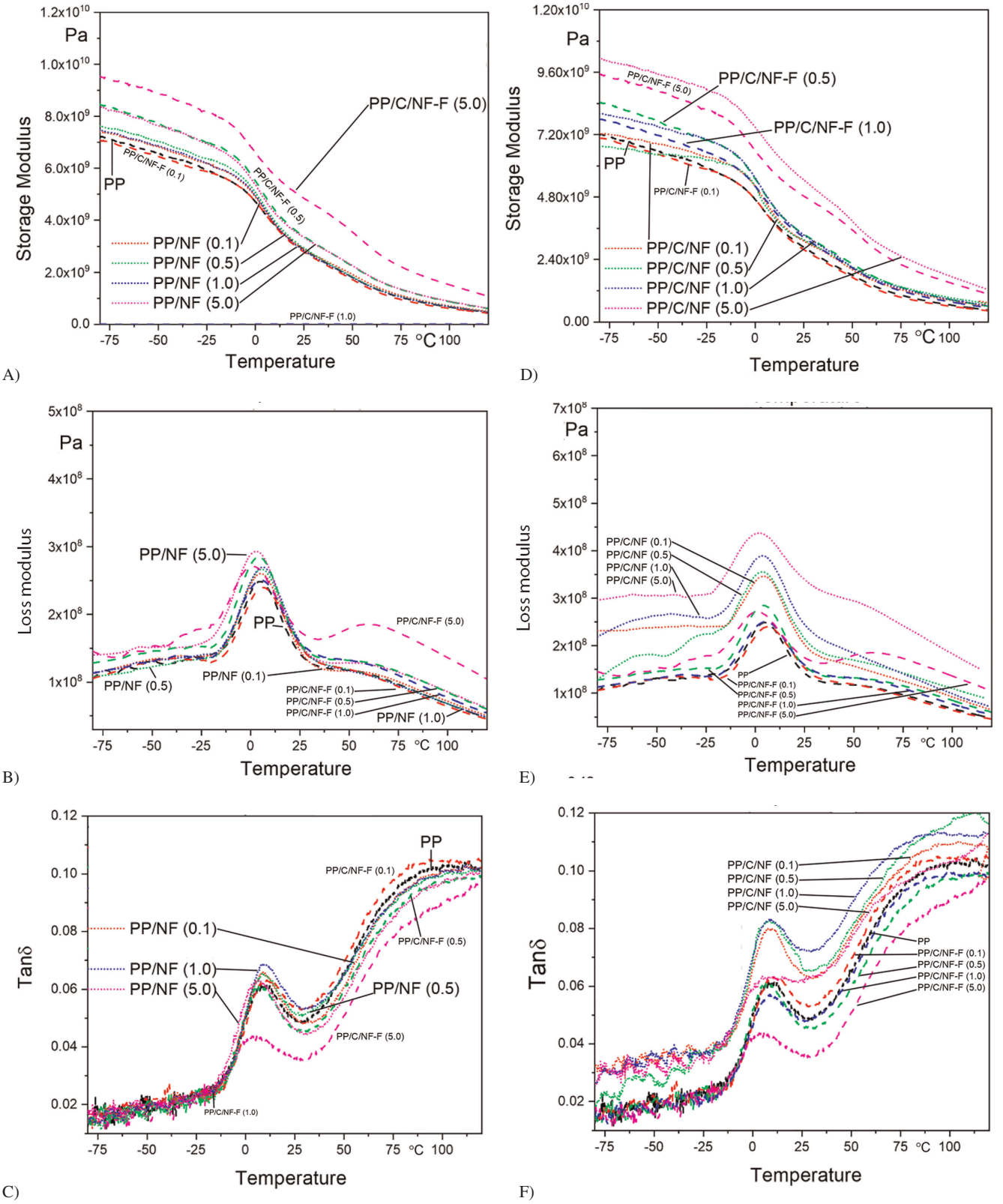

Fig. 8. Variation in storage modulus E′ (A, D), in loss modulus E″ (B, D) and in tan δ (C, F) as as function of temperature PP/NF and PP/C/NF-F composites, respectively

properties obtained. At this composition, rheological percolation was achieved and the greatest increase in Young's modulus (E) and storage modulus (E′) relative to PP recorded. At this composition, the C/NF-F forms an interconnected filler-filler network with the PP, which results in a decrease in crystallinity. However, it was at the 0.1 wt% loading that the greatest increases in toughness (W_b) and ductility (ε_B) were obtained. A highly dispersed and cross-linked C/NF-F to PP resulted in a drastic change in crystal structure, co-crystallization and polymer chain entanglements and therefore a range of matrix properties. This effect of the change in properties can be seen more clearly by plotting normalized values for five key properties, see Fig. 11. The normalized values (X/X_0), where X is some property value of the composite, is divided by the corresponding value for the neat polymer (X_0) and plotted as a function of NF concentration (Kotsilkova et al., 2010) for each composite prepared.

In this instance, the dynamic viscosity (η') at ω = 0.01 592 rads/s, *E′* (from DMTA) at 50 °C, Young's modulus (E), tensile strength (σ) and crystallinity (X_c) values for PP/NF, PP/C/NF and PP/C/NF-F composites were examined. For composites of PP and NF, i.e. without C or functionalization of NF with F, any increase in properties were modest. This is as expected and proves that the addition of slightly polar NF, (i.e. rGO), to PP alone will not yield increased properties due to the incompatibility between the two moieties (filler and matrix) and the propensity for NF to form agglomerations. With the inclusion of C with NF (PP/C/NF composites), E' increases relative to neat PP, but the static tensile properties were unchanged, within experimental error. Additionally, at low frequencies, η' decreases relative to neat PP and a percolated network has not formed. When C is not covalently bound to NF-F, it plays a different role within the polymer matrix. When C is covalently linked to NF-F and dispersed in PP, an increase in E, σ and E' are obtained with increasing C/NF-F loading relative to unfilled PP. Furthermore, for C/NF-F loadings ≤ 1 wt%, X_c also increases relative to neat PP and all other composites, as it is well dispersed in the PP matrix and there are stronger interfacial interactions with the PP matrix.

Sample	T_g (tan δ)	tan δ at T_g	T_g (E″)
PP	8.9	0.06	4.1
PP/NF (0.1)	8.2	0.07	3.8
PP/NF (0.5)	8.5	0.07	4.8
PP/NF (1.0)	8.1	0.07	6.1
PP/NF (5.0)	6.2	0.06	1.1
PP/C/NF (0.1)	9.0	0.08	5.3
PP/C/NF (0.5)	8.4	0.08	2.0
PP/C/NF (1.0)	8.6	0.08	3.6
PP/C/NF (5.0)	5.4	0.06	1.7
PP/C/NF-F (0.1)	9.5	0.06	3.9
PP/C/NF-F (0.5)	6.1	0.06	3.7
PP/C/NF-F (1.0)	7.6	0.06	3.8
PP/C/NF-F (5.0)	4.4	0.04	-1.1

Table 4. Glass transition temperature (T_g) determined from tan δ and E″ plots as a function of temperature, and tan δ values at T_g for neat PP, PP/NF, PP/C/NF and PP/C/NF-F composites

4 Conclusions

Addition of NF to PP resulted in a modest increase in static and dynamic mechanical properties and no rheological percolation threshold. The un-functionalized, polar NF is not well dispersed or distributed in the non-polar PP matrix. However, when the cysteamine functionalized rGO (NF-F) is bound to PP-g-MA (C), interfacial interactions are promoted between NF-F and the PP matrix. When C is not bound to NF-F, C acts more like a plasticizer for the PP. Therefore, for the PP/C/NF-F composites, the covalent attachment between NF-F and the C via cysteamine led to an increase in E, σ and at low C/NF-F loadings significant improvements in W_b and ε_B. Additionally, a rheological percolated network was also formed between 3 and 5 wt% C/NF-F.

The linking covalently of C and NF-F facilitated different interactions between the composite components, including filler-filler, polymer-filler and polymer-polymer, the latter via co-crystallization of the PP chains on PP-g-MA and the bulk PP matrix. The primary mechanism for reinforcement of the PP was the increase in nucleation sites for PP crystallization, which in turn altered the orientation of inter-lamellae slipping during the deformation of the polymer under tension. Functionalization and consequent effective GO dispersion improved load transfer from the matrix to the filler (Castillo et al., 2020).

The crystallization behavior of PP was greatly altered on inclusion of GO, irrespective of whether the GO was functionalized or not. The GO has a strong nucleating effect on PP, preferentially inducing the formation of the α-polymorph and supressing growth of the β-polymorph. The GO initiated heterogeneous nucleation of PP, increasing T_m with increasing NF loading, by up to 10 °C. The super-cooling (ΔT) decreased by up to 17 °C with increasing filler loading.

Cysteamine functionalization of GO in combination with PP-g-MA is effective in assisting dispersion of polar GO in non-polar PP at low loadings (0.1 wt%) only, while at loadings > 0.1 wt%, functionalisation does promote interfacial interaction with a limited effect on dispersion.

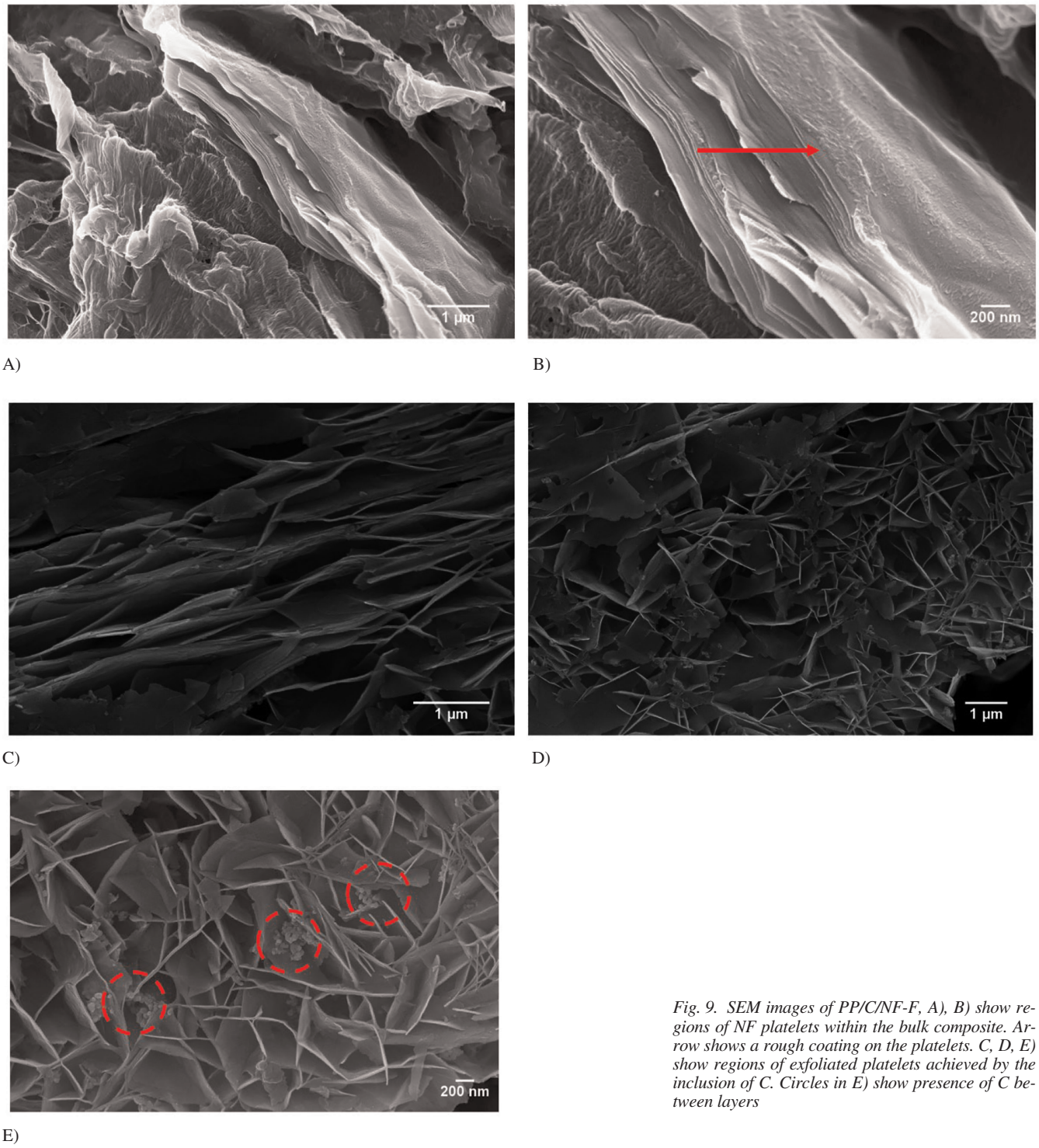

Fig. 9. SEM images of PP/C/NF-F, A), B) show regions of NF platelets within the bulk composite. Arrow shows a rough coating on the platelets. C, D, E) show regions of exfoliated platelets achieved by the inclusion of C. Circles in E) show presence of C between layers

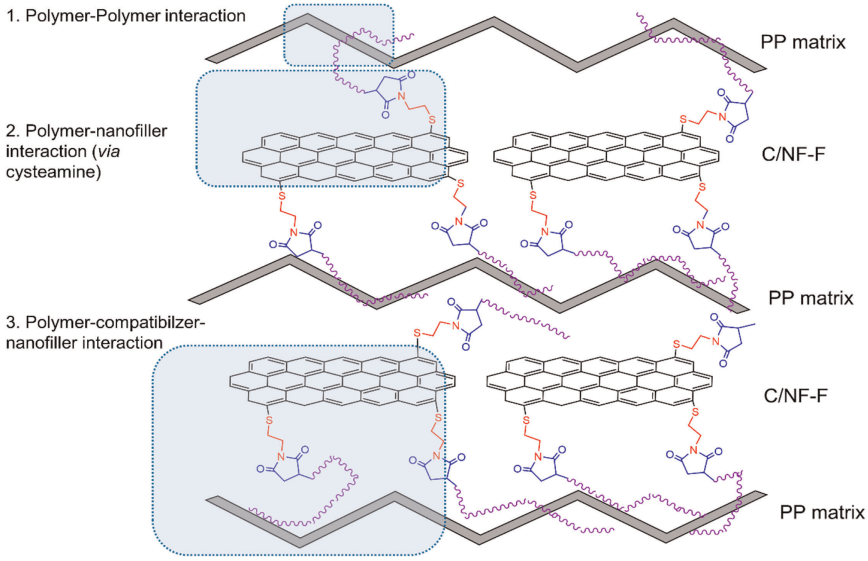

Fig. 10. Schematic representation of the proposed role C plays in 1) polymer-polymer interactions, 2) polymer-NF-F interactions (via cysteamine) and 3) polymer-C/NF-F interaction

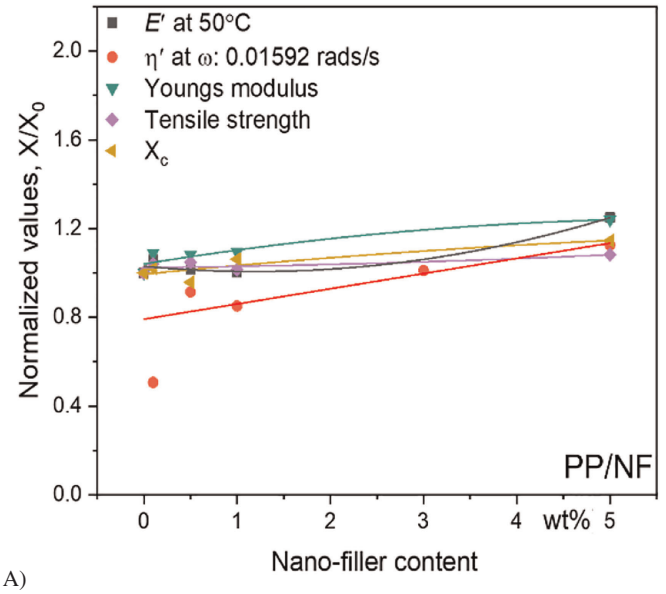

A)

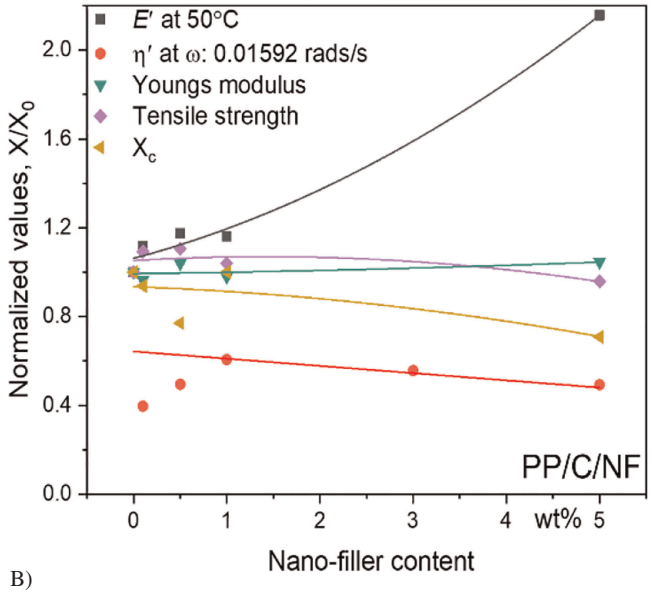

B)

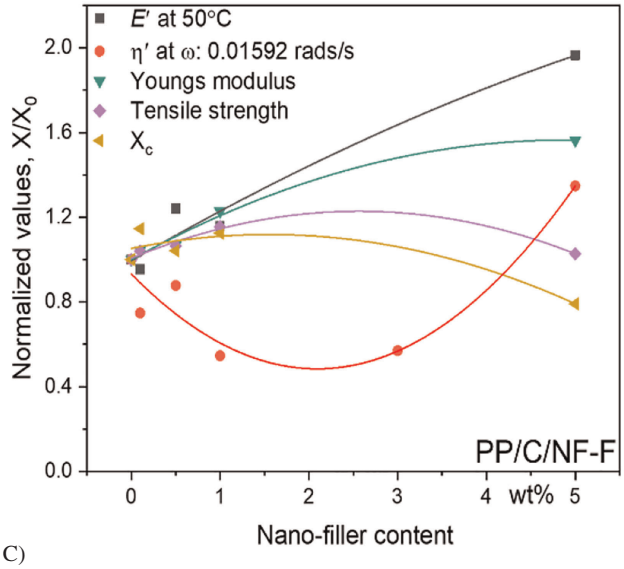

C)

Fig. 11. Normalized values for η′ at ω: 0.01592 rads/s, storage modulus (E') from DMTA at 50°C, Young's modulus (E), tensile strength (σ) and crystallinity (X_c) for A) PP/NF, B) PP/C/NF and C) PP/C/NF-F composites as a function of NF content. Scattered plots fitted to the non-linear line of best fit

References

Abbas, S. S., Kelly, N. L., Patias, G., Hanna J. and McNally, T., "Cysteamine Functionalised Reduced Graphene Oxide Modification of Maleated Poly(propylene)", Polymer, **203**, 122750 (2020a), DOI:10.1016/j.polymer.2020.122750

Abbas, S. S., Rees, G. J., Patias, G., Dancer, C. E. J., Hanna, J. and McNally, T., "In Situ Cross-Linking of Silane Functionalized Reduced Graphene Oxide and Low-Density Polyethylene", ACS Appl. Polym. Mater., **2**, 1897–1908 (2020b), DOI:10.1021/acsapm.0c00115

Ardanuy, M., Velasco, J. J., Antunes, M., Rodriguez-Perez, M. and de Saja, J. A., "Structure and Properties of Polypropylene/Hydrotalcite Nanocomposites", Polym. Compos., **31**, 870–878 (2010), DOI:10.1002/pc.20869

Bai, J.-J., Hu, Zhang, G.-S., Liu, J.-T., Cui, B.-X., Hou, J.-J., Yu, X.-R. and Li, Z.-Z., "Preparation and Rheology of Isocyanate Functionalized Graphene Oxide/Thermoplastic Polyurethane Elastomer Nanocomposites", J. Macromol. Sci., Part B Phys., **58**, 425–441 (2019), DOI:10.1080/00222348.2019.1565102

Benmesli, S., Riahi, F., "Dynamic Mechanical and Thermal Properties of a Chemically Modified Polypropylene/Natural Rubber Thermoplastic Elastomer Blend", Polym. Test., **36**, 54–61 (2014), DOI:10.1016/j.polymertesting.2014.03.016

Castillo, J., Lozano-Garcia, T., Morales-Zamudio, R., López-Barroso, L., Lafleur, J., Karami, P. G., Sanchez-Valdes, S., Martinez-Colunga, S., Rodriguez, G., Perez-Berumen, F., Flores, C. and García, A., "Influence of Graphene-Based Compounds on the Mechanical Toughness and Thermal Stability of Polypropylene", J. Appl. Polym. Sci., **137**, 48258 (2020), DOI:10.1002/app.48258

Chin, S. J., Vempati, S. D., Dawson, P., Knite, M., Linarts, A., Ozols, K. and McNally, T., "Electrical Conduction and Rheological Behavior of Composites of Poly(ε-caprolactone) and MWCNTs", Polymer, **58**, 209–221 (2015), DOI:10.1016/j.polymer.2014.12.034

Chiu, Y.-C., Huang, C.-L. and Wang, C., "Rheological and Conductivity Percolations of Syndiotactic Polystyrene Composites Filled with Graphene Nanosheets and Carbon Nanotubes: A Comparative Study", Compos. Sci. Technol., **134**, 153–160 (2016), DOI:10.1016/j.compscitech.2016.08.016

De Rosa, C., Scoti, M., Di Girolamo, R., de Ballesteros, O. R., Auriemma, F. and Malafronte, A., "Polymorphism in Polymers: A Tool to Tailor Material's Properties", Polym. Cryst., **3**, e10101 (2020), DOI:10.1002/pcr2.10101

Dechant, J.: Polymer Handbook. 3rd Edition, John Wiley & Sons, New York (1990)

Foster, C. W., Down, P. M., Zhang, Y., Ji, X.-B., Rowley-Neale, S. J., Smith, G. C., Kelly, J. P. and Banks, C. E., "3D Printed Graphene Based Energy Storage Devices", Sci. Rep., **7**, 42233 (2017), DOI:10.1038/srep42233

Gupta, J., Wan, C., Haddleton, D. M., and McNally, T., "Plasticisation and Compatibilisation of Poly(propylene) with Poly(lauryl acrylate) Surface Modified MWCNTs", Polymer, **133**, 89–101 (2017), DOI:10.1016/j.polymer.2017.11.025

Harper, D. P., Laborie, M.-P. G. and Wolcott, M. P., "The Impact of Polypropylene-Graft-Maleic Anhydride on the Crystallization and Dynamic Mechanical Properties of Isotactic Polypropylene", J. Appl. Polym. Sci., **111**, 753–758 (2009), DOI:10.1002/app.29100

Hsiao, M.-C., Liao, S.-H., Lin, Y.-F., Wang, C.-A., Pu, N.-W., Tsai, H.-M. and Ma, C.-C. M., "Preparation and Characterization of Polypropylene-Graft-Thermally Reduced Graphite Oxide with an Improved Compatibility with Polypropylene-Based Nanocomposite", Nanoscale, **3**, 1516–1522 (2011), DOI:10.1039/c0nr00981d

Huo, H., Jiang, S., An, L. and Feng, J., "Influence of Shear on Crystallization Behavior of the β Phase in Isotactic Polypropylene with β-Nucleating Agent", Macromolecules, **37**, 2478–2483 (2004), DOI:10.1021/ma0358531

Juhász, P., Varga, J., Belina, K. and Belina, G., "Efficiency of β-Nucleating Agents in Propylene/α-Olefin Copolymers", J. Macromol. Science, Part B Phys., **41**, 1173–1189 (2002), DOI:10.1081/MB-120013090

Kalantari, B., Mojtahedi, M. R. M., Sharif, F. and Rahbar, R. S., "Effect of Graphene Nanoplatelets Presence on the Morphology, Structure, and Thermal Properties of Polypropylene in Fiber Melt-Spinning Process", Polym. Compos., **36**, 367–375 (2015a), DOI:10.1002/pc.22951

Kalantari, B., Mojtahedi, M. R. M., Sharif, F. and Rahbar, R. S., "Flow-Induced Crystallization of Polypropylene in the Presence of Graphene Nanoplatelets and Relevant Mechanical Properties in Nanocompsoite Fibres", Composites Part A, **76**, 203–214 (2015b), DOI:10.1016/j.compositesa.2015.05.028

Khare, R. A., Bhattacharyya, A. R. and Kulkarni, A. R., "Melt-Mixed Polypropylene/Acrylonitrile-Butadiene-Styrene Blends with Multiwall Carbon Nanotubes: Effect of Compatibilizer and Modifier on Morphology and Electrical Conductivity", J. Appl. Polym. Sci., **120**, 2663–2672 (2011), DOI:10.1002/app.33371

Kotsilkova, R., Ivanov, E., Krusteva, E., Silvestre, C., Cimmino S. and Duraccio, D., "Isotactic Polypropylene Composites Reinforced with Multiwall Carbon Nanotubes, Part 2: Thermal and Mechanical Properties Related to the Structure", J. Appl. Polym. Sci., **115**, 3576–3585 (2010), DOI:10.1002/app.30413

Lertwimolnun, W., Vergnes, B., "Influence of Compatibilizer and Processing Conditions on the Dispersion of Nanoclay in a Polypropylene Matrix", Polymer, **46**, 3462–3471 (2005), DOI:10.1016/j.polymer.2005.02.018

Létoffé, A., García-Rodríguez, S., Hoppe, S., Canilho, N., Godard, O., Pasc, A., Royaud, I. and Ponçot, M., "Switching from Brittle to Ductile Isotactic Polypropylene-g-Maleic Anhydride by Crosslinking with Capped-End Polyether Diamine", Polymer, **164**, 67–78 (2019), DOI:10.1016/j.polymer.2019.01.015

Li, C.-Q., Zha, J.-W., Long, H.-Q., Wang, S.-J., Zhang, D.-L. and Dang, Z.-M., "Mechanical and Dielectric Properties of Graphene Incorporated Polypropylene Nanocomposites Using Polypropylene-Graft-Maleic Anhydride as a Compatibilizer", Compos. Sci. Technol., **153**, 111–118 (2017), DOI:10.1016/j.compscitech.2017.10.015

Liu, Z., Zheng, G., Dai, K., Liu, C. and Shen, C., "Simultaneously Improving Tensile Strength and Toughness of Melt-Spun β-Nucleated Isotactic Polypropylene Fibers", J. Appl. Polym. Sci., **133**, (2016), DOI:10.1002/app.43454

Lv, C., Xue, Q., Xia, D., Ma, M., Xie, J. and Chen, H., "Effect of Chemisorption on the Interfacial Bonding Characteristics of Graphene–Polymer Composites", J. Phys. Chem. C, **114**, 6588–6594 (2010), DOI:10.1021/jp100110n

Martínez-Colunga, J. G., Sanchez-Valdes, S., Ramos-deValle, L. F., Perez-Camacho, O., Ramirez-Vargas, E., Benavides-Cantú, R., Avila-Orta, C. A., Cruz-Delgado, V. J., Mata-Padilla, J. M., Lozano-Ramírez, T. and Espinoza-Martínez, A. B., "Aniline-Modified Polypropylene as a Compatibilizer in Polypropylene Carbon Nanotube Composites", Polym. Plast. Technol. Eng., **57**, 1360–1366 (2018), DOI:10.1080/03602559.2017.1381251

McClory, C., McNally, T., Baxendale, M., Pötschke, P., Blau, W. and Ruether, M., "Electrical and Rheological Percolation of PMMA/MWCNT Nanocomposites as a Function of CNT Geometry and Functionality", Eur. Polym. J., **46**, 854–868 (2010), DOI:10.1016/j.eurpolymj.2010.02.009

Menyhárd, A., Faludi, G. and Varga, J., "β-Crystallisation Tendency and Structure of Polypropylene Grafted by Maleic Anhydride and its Blends with Isotactic Polypropylene", J. Therm. Anal. Calorim., **93**, 937–945 (2008), DOI:10.1007/s10973-007-8569-7

Mun, S. C., Kim, M., Prakashan, K., Jung, H. J., Son, Y. and Park, O. O., "A New Approach to Determine Rheological Percolation of Carbon Nanotubes in Microstructured Polymer Matrices", Carbon, **67**, 64–71 (2014), DOI:10.1016/j.carbon.2013.09.056

Murthy, N. S., "Chapter 2 X-Ray Diffraction from Polymers", in Polymer Morphology, Guo, Q. (Ed.),Wiley, New Jersey, p. 14–36 (2016), DOI:10.1002/9781118892756.ch2

Nobile, M. R., "Chapter 15 Rheology of Polymer–Carbon Nanotube Composites Melts", in Polymer–Carbon Nanotube Composites, McNally, T., Pötschke, P. (Eds.), Woodhead Publishing, Oxford, p. 428–481 (2011), DOI:10.1533/9780857091390.2.428

Parija, S., Bhattacharyya, A. R., "Role of Interfacial Interactions to Control the Extent of Wrapping of Polymer Chains on Multi-Walled Carbon Nanotubes", RSC Advances, **6**, 42334–42346 (2016), DOI:10.1039/C6RA06258J

Potts, J. R., Dreyer, D. R., Bielawski, C. W. and Ruoff. R. S.,"Graphene-Based Polymer Nanocomposites", Polymer, **52**, 5 – 25 (2011), DOI:10.1016/j.polymer.2010.11.042

Sánchez-Valdes, S., Zapata-Domínguez, A. G., Martinez-Colunga, J. G., Mendez-Nonell, J., Ramos de Valle, L. F., Espinoza-Martinez, A. B., Morales-Cepeda, A., Lozano-Ramirez, T., Lafleur, P. G. and Ramirez-Vargas, E., "Influence of Functionalized Polypropylene on Polypropylene/Graphene Oxide Nanocomposite Properties", Polym. Compos., **39**, 1361 – 1369 (2018), DOI:10.1002/pc.24077

Song, N., Yang, J., Ding, P., Tang, S., Liu, Y. and Shi, L., "Effect of Covalent-Functionalized Graphene Oxide with Polymer and Reactive Compatibilization on Thermal Properties of Maleic Anhydride Grafted Polypropylene", Ind. Eng. Chem. Res., **53**, 19951 – 19960 (2014), DOI:10.1021/ie5031985

Sun, X., Liu, Z., Welsher, K., Robinson, J. T., Goodwin, A., Zaric, S. and Dai, H., "Nano-Graphene Oxide for Cellular Imaging and Drug Delivery", Nano Res., **1**, 203 – 212 (2008), DOI:10.1007/s12274-008-8021-8

Van Vlack, L. H.: Elements of Materials Science and Engineering, 6 Edition, Addison-Wesley, Michigan (1989)

Yetgin, S. H.,"Tribological Properties of Compatabilizer and Graphene Oxide-Filled Polypropylene Nanocomposites", Bull. Mater. Sci., **43**, 89 – 96 (2020), DOI:10.1007/s12034-020-2061-4

Yuan, B., Bao, C., Song, L., Hong, N., Liew, K. M. and Hu, Y., "Preparation of Functionalized Graphene Oxide/Polypropylene Nanocomposite with Significantly Improved Thermal Stability and Studies on the Crystallization Behavior and Mechanical Properties", Chem. Eng. J., **237**, 411 – 420 (2014), DOI:10.1016/j.cej.2013.10.030

Zheng, Q., Xue, Q., Yan, K., Hao, L., Li, Q. and Gao, X., "Investigation of Molecular Interactions between SWNT and Polyethylene/Polypropylene/Polystyrene/Polyaniline Molecules", J. Phys. Chem. C, **111**, 4628 – 4635 (2007), DOI:10.1021/jp066077c

Acknowledgements

SA thanks EPSRC and Jaguar Land Rover for funding an iCASE PhD studentship.

Date received: December 11, 2020
Date accepted: February 04, 2021

Bibliography
DOI 10.1515/ipp-2020-4079
Intern. Polymer Processing XXXVI (2021) 3; page 297 – 313

ISSN 0930-777X · 2195-8602